pubs.acs.org/jasms Research Article

Formation of Carbohydrate—Metal Adducts from Solvent Mixtures during Electrospray: A Molecular Dynamics and ESI-MS Study

Emvia I. Calixte, O. Tara Liyanage, Darren T. Gass, and Elyssia S. Gallagher*



Cite This: J. Am. Soc. Mass Spectrom. 2021, 32, 2738-2745



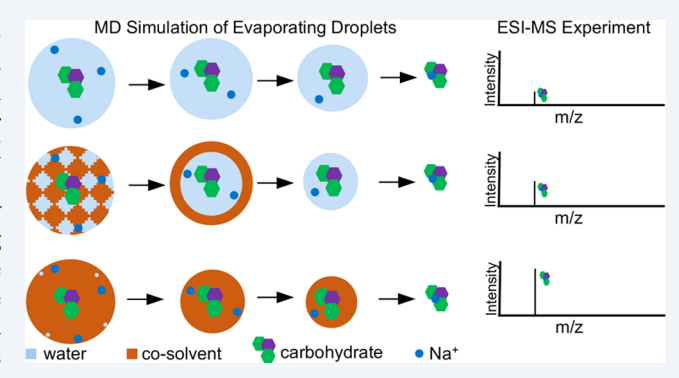
ACCESS I

III Metrics & More

Article Recommendations

Supporting Information

ABSTRACT: Electrospray ionization (ESI) is frequently used to produce gas-phase ions for mass spectrometry (MS)-based techniques. The composition of solvents used in ESI-MS is often manipulated to enhance analyte ionization, including for carbohydrates. Moreover, to characterize analyte structures, ESI has been coupled to hydrogen/deuterium exchange, ion mobility, and tandem MS. Therefore, it is important to understand how solvent composition affects the structure of carbohydrates during and after ESI. In this work, we use molecular dynamics to simulate the desolvation of ESI droplets containing a model carbohydrate and observe the formation of carbohydrate adducts with metal ions. Molecular-level details on the effects of formulating mixtures of water, methanol, and acetonitrile to achieve enhanced ionization



are presented. We complement our simulations with ESI-MS experiments. We report that when sprayed from aqueous mixtures containing volatile solvents, carbohydrates ionize to form metal—ion adducts rapidly due to rapid solvent evaporation rather than changes in the ionization mechanism. We find that when sprayed from solvent mixtures, carbohydrates are primarily solvated by water due to the migration of more volatile solvents to the surface of the droplet. Ultimately, the structure of the carbohydrate varies depending on its solvent environment, as inter- and intramolecular interactions are affected. We propose that solvents with 25% or more water may be used to enhance the ionization of carbohydrates with minimal effect on the structure during and after ESI.

1. INTRODUCTION

Glycans, the carbohydrate moieties of glycoproteins and glycolipids, are an important component in mammalian cell surfaces, as they play significant roles in molecular recognition and signaling.1 Additionally, glycans serve as markers for many diseases, ^{2,3} as their structures change during disease onset and progression. Mass spectrometry (MS) methods such as ion mobility (IM)-MS and tandem MS (MS/MS) are commonly used to characterize glycans in the gas phase,^{4,5} while in-electrospray ionization (ESI) hydrogen/deuterium exchange (HDX)-MS has been used to analyze structures of solvated carbohydrates.^{6,7} Since carbohydrates are uncharged molecules, ESI is often used with MS to transfer carbohydrates from solution to the gas phase as adducts with ions. Parameters such as analyte concentration, electrolyte concentration, flow rate, electric potential, and choice of solvent are often manipulated to optimize the ionization efficiency of glycans during ESI-MS experiments. Methanol or acetonitrile, often in mixtures with water, have been employed to increase the analyte signal, 8,9 improving the ionization efficiency.

Molecular dynamics (MD) simulations have been an invaluable computational approach to both investigate carbohydrate structures in water and model the evaporation of droplets. Two of the primary mechanisms of ionization during ESI are the charged residue model (CRM) and the ion

evaporation mechanism (IEM).¹⁶ The CRM is characterized by total solvent evaporation from a droplet resulting in the droplets' residual charge adducting to the analyte. Alternatively, the IEM is characterized by ejection of charged analytes from evaporating droplets when Coulombic repulsion overcomes the surface tension of the solvent. Recently, we established the mechanism of ionization of carbohydrates from water during ESI.¹¹ We revealed that interactions between the carbohydrate and water played a significant role in the energetic ability for an analyte to be released from an evaporating droplet. The ionization mechanisms for unmodified and permethylated (modified) carbohydrates differed because of those interactions. The CRM was observed for unmodified carbohydrates and resulted in poorer ionization compared to permethylated carbohydrates, which experienced the IEM and had enhanced ionization.

Received: June 4, 2021
Revised: October 4, 2021
Accepted: October 21, 2021
Published: November 4, 2021





Table 1. Starting Molecular Compositions in Droplet Systems with a Radius of 3 nm

		Water/Methanol Systems					Water/Acetonitrile Systems				
component	no cosolvent 100% water	75% water	50% water	25% water	10% water	1% water	75% water	50% water	25% water	10% water	1% water
water	3760	2766	1844	922	369	37	2766	1844	922	369	37
cosolvent	-	394	788	1182	1419	1560	312	624	936	1123	1235
Na ⁺	20	15	13	12	11	10	16	13	13	13	12

Solvent mixtures containing organic additives enhance the ionization of glycans.^{8,9} Given our earlier findings that carbohydrate ionization efficiencies were based on different ionization mechanisms, we sought to determine the ionization mechanism from mixed solvents. We investigated whether the strength of the interactions with mixed solvents would be reduced, such that it would be more energetically favorable for the carbohydrate to coordinate to the metal and be pushed out of the droplet through Coulombic repulsion, as in the IEM. Alternatively, the mixed solvents could result in a faster evaporative rate and thus faster coordination with the metal, while maintaining ionization by the CRM. Additionally, we investigated what ratio of water to organic solvent would provide a reasonable improvement in the ionization efficiency without changing the solvated or gas-phase structures of the carbohydrate. An answer to this question is critical for determining the limitations of using solvent mixtures for ESI-MS methods that examine carbohydrate structures.

In the present work, using MD simulations and ESI-MS experiments, we investigate the ionization of the carbohydrate melezitose, which is a trisaccharide and a model glycan, in solvents with varying compositions of water, methanol, and acetonitrile. We determine the consequences of solvent composition on the ESI mechanism, ionization efficiency, and carbohydrate structure during and after ESI. Overall, this work provides a fundamental, molecular description of the ESI process for carbohydrates from solvent mixtures.

2. METHODS

2.1. Molecular Dynamics (MD) Simulations. MD simulations were performed to investigate the effects of solvent variation on electrospray ionization of melezitose. We used systems with different molecular compositions: (i) evaporating droplets and (ii) bulk systems, both containing melezitose in methanol- or acetonitrile-based solvent mixtures. The structure of melezitose was first obtained from the zinc database¹⁷ and optimized using DFT calculations at the B3LYP/6-311++G(d,p) level (Becke three-parameter exchange correlation functional with diffuse and polarization functions) using Gaussian09.18 Topology files based on parameters from the CHARMM36 force field were generated using the Paramchem/CGenFF-4.0^{20,21} server for TIP3P water and all-atom models for melezitose, methanol, and acetonitrile. Results from MD simulations are force field dependent, so the CHARMM force field was selected for its reproducibility of experimental results when modeling carbohydrates and carbohydrate-containing biomolecules. TIP3P water was used because the CHARMM force field was parametrized for the TIP3P water model. MD simulations were performed using the GROMACS package.²²

Bulk systems $(4 \times 4 \times 4 \text{ nm}^3 \text{ cubic boxes with } 400 \text{ molecules})$ of pure water, pure methanol, and pure acetonitrile were simulated to determine density at the equilibrium temperature of 323 K. Based on the bulk densities, the

number of solvent molecules for a given volume fraction in the mixed solvent systems was determined for droplets with 3 nm radii. We selected 3 nm radii because it has been suggested that the ionization of charged analytes through IEM occurs in nanodroplets with radii less than 10 nm. 23 Additionally, droplets with radii of 3 nm have several layers of solvent molecules around the carbohydrate, enabling the investigation of solvation and evaporation. Finally, this size provides a reasonable computational expense. Droplets with radii of 2-3 nm are often used to simulate evaporating droplets.^{7,10-12} Table 1 contains the starting quantities of each molecule for evaporating droplets. Droplets of water/methanol and water/ acetonitrile mixtures were built using Packmol.²⁴ System compositions were pure water, 75:25, 50:50, 25:75, 10:90, and 1:99 volume %/volume % ratios of water/cosolvent, where the cosolvent was methanol or acetonitrile. Herein, these systems will be referred to as 100%, 75%, 50%, 25%, 10%, and 1% water in methanol or acetonitrile. Na+ ions were selected as the charge carriers to reproduce simulations of droplets in positiveion mode. The number of Na+ ions was calculated based on the critical limit of Rayleigh stability,²⁵ which is the balance between the opposing forces of surface tension and Coulomb repulsion among ions of a charged droplet. The number of ions to be added to the droplets was determined from the Rayleigh equation, using surface tension values for water/methanol and water/acetonitrile mixtures. The surface tension values (in N/ m) for water and water/methanol mixtures were 0.068 (100% water), 0.041 (75% water), 0.030 (50% water), 0.023 (25% water), 0.021 (10% water), and 0.020 (1% water or pure methanol) at 323 K.²⁶ The surface tension values for water/ acetonitrile mixtures were 0.040 (75% water), 0.033 (50% water), 0.030 (25% water), and 0.030 (10% water) at 298 K and 0.026 (1% water or pure acetonitrile at 323 K).²

The small (3 nm) droplets were placed in large systems (1000 nm in x, y, and z dimensions) consisting mostly of vacuum, to reproduce a pseudo-PBC²⁸ environment. The steepest energy minimization was done, followed by NVT equilibration of the droplets before evaporation. The Leapfrog integrator²⁹ with a time step of 1 fs was employed within the Verlet scheme.³⁰ The Nosé-Hoover thermostat^{31,32} was used to regulate the temperature to 323 K with a time constant of 1 ps. While solvent evaporated from the droplet and solvated ions were ejected, Konermann's code^{33,10} was used to adjust for the change in the center of the droplet and to remove evaporated solvent from the system in several separate MD runs that are then combined through trajectory stitching. Evaporated solvent, which had moved beyond 10 nm of the center of mass of the droplet, was removed. The temperature of the system was re-equilibrated between runs to compensate for evaporative cooling.³⁴

Simulations in cubic boxes with periodic boundary conditions in all directions were also performed on systems with similar numbers of melezitose and mixed solvent but without ions. These systems represent our bulk mixed solvent

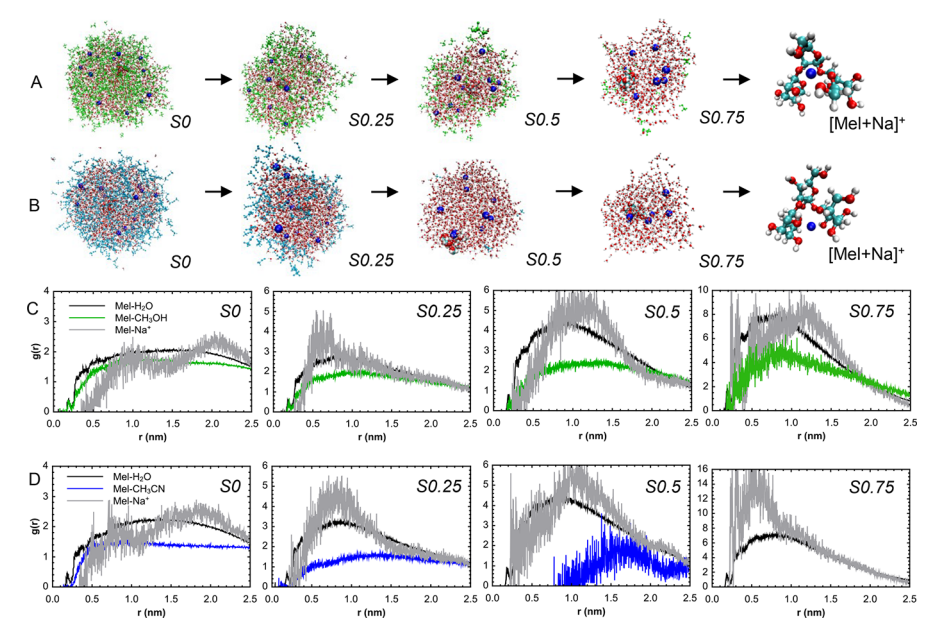


Figure 1. Representative snapshots showing progression of solvent distributions in droplets containing 50:50 (A) water/methanol and (B) water/acetonitrile at different stages of evaporation: S0 (post equilibration), S0.25 (25% solvent evaporation), S0.5 (50% solvent evaporation), S0.75 (75% solvent evaporation), and complete dryness with the melezitose adducted to a sodium ion, [Mel + Na]⁺. Snapshots have been zoomed in to observe molecular details and are not to scale. The atom colors for melezitose and water molecules are red for oxygen, white for hydrogen, and cyan for carbon. Methanol molecules are green; acetonitrile molecules are blue; and Na⁺ ions are blue spheres. Radial distribution profiles are shown between melezitose and water (Mel–H₂O), melezitose and methanol (Mel–CH₃OH), melezitose and acetonitrile (Mel–CH₃CN), and melezitose and sodium ions (Mel–Na⁺) in 50:50 (C) water/methanol and (D) water/acetonitrile.

simulations. No ions were added, as these systems in positiveion mode would have a net charge, which is not appropriate for MD systems using PME decomposition. Bulk systems were equilibrated using the previously mentioned thermodynamic parameters but contained an additional NVT production run of 30 ns of simulation time. Throughout this work, reported errors and error bars correspond to the standard deviation of ten replicate trials for MD simulations. A Students' t test was used for statistical comparisons.

2.2. Materials. Melezitose was purchased from Sigma (St. Louis, MO); sodium chloride was from VWR International Inc. (Radnor, PA); and methanol and acetonitrile were from Fisher Scientific (Waltham, MA). All chemicals were used without further purification. Nanopure water was acquired from a Purelab Flex 3 purification system from Elga, Veolia Environment S. A. (Paris, France).

2.3. ESI-MS. ESI-MS data were acquired on an Orbitrap Discovery MS (Thermo-Fisher Scientific, Waltham, MA). Experiments utilized spray voltage of 3.5 kV, capillary temperature of 300 °C, auxiliary gas (N_2) of 0 arb units, sheath gas (N_2) of 12 arb units, and infusion flow rate of 20 μ L/min. Solutions of melezitose (100 μ M) and sodium chloride were prepared at a 1:1 molar ratio in each of the solvent compositions of 1%, 10%, 25%, 50%, 75%, and 100% water with organic solvent, methanol, or acetonitrile. ESI-MS experiments were performed in triplicate.

3. RESULTS AND DISCUSSION

3.1. Carbohydrates in Mixtures with 25% or More Water Experience Demixing and Ionize by the CRM. Our first goal was to determine the mechanism of ionization of carbohydrates from droplets with mixed solvent compositions. From the trajectories of MD simulations, we observed that the carbohydrate remained in the droplet while the solvent mixture

evaporated, a process characteristic of the CRM. 11 For droplets with high proportions of water (25% or more), the organic component evaporated first, followed by complete evaporation of the water molecules, resulting in an adduct of the carbohydrate with sodium ions, represented as [Mel + Na]+. Figure 1 contains snapshots of the overall arrangement of molecules in the droplets with starting compositions of 50:50 water, with either methanol (A) or acetonitrile (B). The snapshots illustrate four stages of total solvent evaporation: S0 (post equilibration), S0.25 (25% solvent evaporation), S0.5 (50% solvent evaporation), and S0.75 (75% solvent evaporation). Figures 1A and 1B show that carbohydrates in the interior of the droplet are increasingly solvated with water, as methanol or acetonitrile migrate to the droplet surface where they evaporate at greater rates than water molecules. This behavior of the solvents, characterized by water enrichment or organic component depletion, is described as demixing.³⁵ The Supporting Information (Figures S1 and S2) contains snapshots of droplet evaporation for all systems. Similar demixing behavior was observed for the other solvent mixtures with 75% and 25% water compositions.

The effects of demixing of droplets with 10% water were not as prominent as that of droplets with 25% or more water, even at the latest stages of evaporation. For example, at 75% evaporation (S0.75), melezitose in droplets with 25% water is mostly solvated with water, but melezitose in droplets with 10% water is solvated with both water and methanol or acetonitrile. At 90% evaporation (S0.9), melezitose in droplets with 10% water are still solvated differently from droplets with 25% water. Specifically, there are only a few methanol molecules in the droplet for 25% water in methanol systems, and there are no acetonitrile molecules present in droplets with 25% water in acetonitrile systems at 90% evaporation. In contrast, droplets with 10% water in methanol or acetonitrile

mostly contain methanol or acetonitrile at 90% evaporation. However, while these droplets with 90% methanol or acetonitrile mostly contain cosolvent, there are still some water molecules present in the solvation shell of melezitose. This is in contrast to droplets with 1% water that are only solvated with cosolvent and did not experience demixing.

To quantify the distribution of solvent and ions around the melezitose molecule at the four evaporation time points, we obtained radial distribution functions (RDFs) presented in panels C and D (Figure 1), according to

$$g_{AB}(r) = \frac{\langle \rho_{B}(r) \rangle}{\langle \rho_{B} \rangle_{local}} = \frac{1}{\langle \rho_{B} \rangle_{local} N_{A}} \sum_{i \in A}^{N_{A}} \sum_{i \in B}^{N_{B}} \frac{\delta(r_{ij} - r)}{4\pi r^{2}}$$
(1)

where $\langle \rho_{\rm B}(r) \rangle$ is the particle density of molecule type B at a distance of r from molecule A, with $\langle \rho_{\rm B} \rangle_{\rm local}$ as the particle density of molecule type B averaged over distances from A. An increase in the height of the RDF profiles is due to an increase in the local density of molecule type B in the droplet, relative to a decreasing overall system density. The center of mass of the carbohydrate was selected as the reference point for A. Oxygen atoms from water and methanol and a carbon atom from acetonitrile were selected as the B reference point. Figure 1C contains RDFs between melezitose and water (Mel-H₂O), melezitose and methanol (Mel-CH₃OH), or melezitose and sodium ions (Mel-Na⁺) at four stages in the evaporation process. Figure 1D contains the corresponding RDFs between melezitose and water (Mel-H₂O), melezitose and acetonitrile (Mel-CH₃CN), and melezitose and sodium ions (Mel-Na⁺).

For both methanol and acetonitrile droplets, as evaporation progresses, the distribution between melezitose and solvents evolves in a manner which reflects demixing. For example, the maximum in the RDF profile for the melezitose-methanol distribution (green traces) becomes more prominent and shifts to larger r values with time (r > 0.5), indicating that the methanol molecules are moving to the periphery of the droplet. For similar evaporation points in water-acetonitrile droplets (Mel-CH₃CN), the distribution patterns are similar to methanol, with the acetonitrile molecules increasingly concentrated at the droplet surface with time. With less acetonitrile cosolvent in water/acetonitrile droplets, compared to methanol in water/methanol droplets of the same radius. there are less acetonitrile molecules at half solvent evaporation than in the methanol droplets, and these acetonitrile molecules are all at the surface of the droplet (panels B and D at S0.5).

The number of solvent molecules or Na^+ ions (C_n) within the first solvation shell of the carbohydrate was obtained by integrating the RDFs. The first solvation shell is a layer of solvent which is one solvent molecule thick. Solvation numbers for melezitose-water and melezitose-cosolvent pairs are presented in Figure 2. In systems with 100% water, the solvation between melezitose and water decreases with solvent evaporation (panels A/E, black trace). At 25% solvent evaporation (S0.25, panel A black trace), the carbohydrate is surrounded by 22 ± 6 water molecules. In 75% water droplets, the solvation number to water increases to a value comparable to that of 100% water at about 25% evaporation (S0.25, panel A green trace and panel E blue trace). At this time point (S0.25), demixing has occurred. For droplets with 25% and 10% water in methanol, there is also a slight increase in coordination to water (green trace) with increasing evaporation. Except for 1% water droplets, coordination to water increases, as demixing occurs.

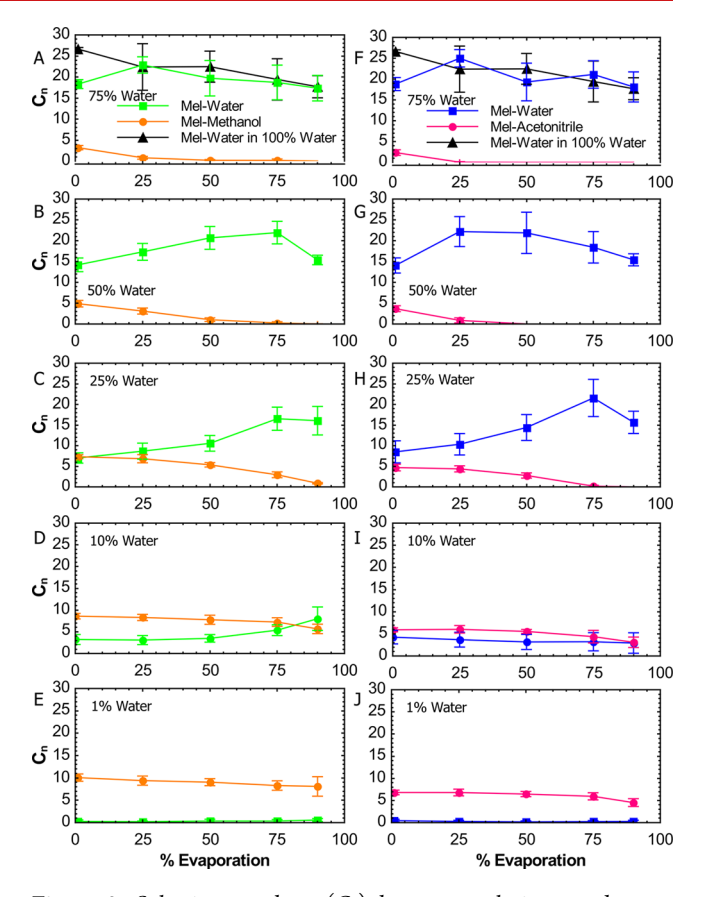


Figure 2. Solvation numbers (C_n) between melezitose and water (Mel–water), melezitose and methanol (Mel–methanol), and melezitose and acetonitrile (Mel–acetonitrile), in methanol droplets (A to E) and acetonitrile droplets (F to J) are plotted as a function of solvent evaporation.

For systems with proportions of water of 50%, the number of water molecules within the first solvation shell is lower for the methanol droplets than for the acetonitrile droplets (p <0.05). The melezitose to water solvation numbers (Melwater) were 17 ± 2 water molecules for 50% water in methanol and 22 \pm 4 water molecules for 50% water in acetonitrile at S0.25. This is likely a result of methanol hydrogen bonding to melezitose, a matter which we will discuss below. However, the difference in Mel-water solvation numbers was not significantly different when comparing methanol to acetonitrile cosolvents in the solvent mixtures with 10%, 25%, or 75% water (p > 0.05). Specifically, the solvation numbers in 10% water droplets at S0.25 were 3 ± 1 and 4 ± 2 in methanol and acetonitrile, respectively. The solvation numbers in 25% water droplets at S0.25 were 9 \pm 2 and 10 \pm 3 in methanol and acetonitrile, respectively. For the 75% water droplets at S0.25, the Mel-water solvation numbers were 23 \pm 2 and 25 \pm 2 in methanol and acetonitrile, respectively.

For all droplets, there are more methanol molecules within the solvation shell of melezitose compared to the number of acetonitrile molecules. For example, the solvation number within the solvation shell of melezitose in 1% water mixtures is 9 ± 1 for methanol and 6.8 ± 0.8 for acetonitrile droplets (p<0.05). This difference is due to the aforementioned hydrogen bonding interactions between melezitose and methanol. Trends in the coordination numbers of melezitose to ions are presented in the Supporting Information (Figure S3).

3.2. Increasing the Proportion of Organic Cosolvent Improves Ionization Efficiency. Our results show a faster evaporative rate for solvent mixtures of decreasing water concentrations and, consequently, a decrease in time for carbohydrate ionization. Figure 3 shows the normalized rate of

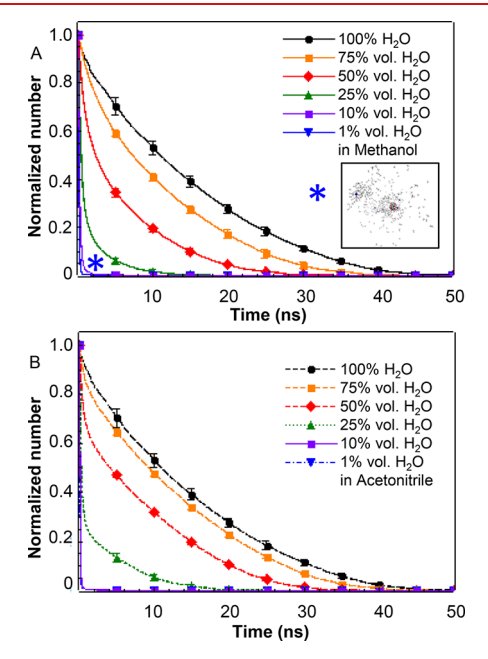


Figure 3. Normalized evaporation of total solvent with time from droplets containing one melezitose molecule and methanol (A) or acetonitrile (B) for various solvent/cosolvent compositions. Inset of (A) presents a snapshot of droplet evaporation observed for some systems with 1% water. Droplet sizes are not to scale. The normalized number of solvent molecules for a given time point was obtained by dividing the current number of solvent molecules by the starting number. Each droplet has a starting radius of 3 nm with a number of Na⁺ ions at the Rayleigh charge limit.

total solvent (water + cosolvent) evaporation for droplets with decreasing water compositions in methanol (panel A) or acetonitrile (panel B). Normalization was done by dividing the number of solvent molecules for a given time point by the starting number of solvent molecules in the droplet. As the volume percent of water decreases from 100% to 1% in both methanol and acetonitrile, the evaporative rate increases. This is expected considering (1) the higher volatility of methanol and acetonitrile versus water and (2) the reduction in the surface tension of the droplets, which allow for faster evaporation of solvent.

Our results also show that the evaporative rate of water/methanol mixtures is faster than that of water/acetonitrile mixtures of the same % water composition. This difference in evaporative rate is most apparent for droplets with 25% and 50% water (Figure 3, green and red traces). The dramatic drop in normalized number of solvent molecules for 1% water and 10% water droplets (blue and purple traces) is due to the inherently fast evaporative rate of methanol or acetonitrile (see inset of Figure 3A). In the 1% water droplets, as the droplet evaporates, the melezitose molecule is solvated with a small number of organic molecules, and this is recorded as a significant drop in solvation. The enhanced evaporation and decomposition of the droplets coincide with the improved ionization that we obtain from ESI-MS experiments. Figure 4 presents the intensity of gas-phase adducts of melezitose with

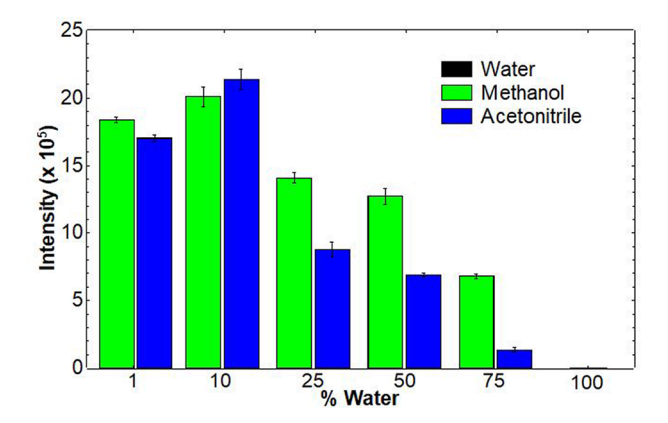


Figure 4. Ionization intensities of melezitose—sodium adducts obtained from ESI-MS experiments in solutions of melezitose (100 μ M) and sodium chloride in solvent compositions of 1%, 10%, 25%, 50%, 75%, and 100% water with methanol or acetonitrile.

sodium ([Mel + Na]⁺). Higher intensity values are reflective of higher ionization efficiencies. The black bar corresponds to the ionization intensity of [Mel + Na]⁺ adducts produced from droplets of 100% water, while the green and blue bars correspond to adducts produced from mixtures of water with methanol or acetonitrile, respectively. As the proportion of water in the mixtures decreases, from 100% water, there is a marked increase in the ionization efficiency reflected by the increasing intensities. The greatest intensities were obtained for solutions with 10% water in methanol or acetonitrile. Generally, the ionization efficiency is greater for methanol mixtures than for acetonitrile.

3.3. Carbohydrates Experience Different Hydrogen Bonding in Solvents with Decreasing Water Concentration. To investigate the hydrogen-bonding interactions involving melezitose in environments with different solvents, we initially examined the carbohydrate in bulk systems (a fully solvated box). Figure 5A presents the number of intermolecular hydrogen bonds $(N_{\rm HB})$ between melezitose and water (Mel-H₂O) and between melezitose and methanol (Mel-methanol) in systems with increasing percentages of water.

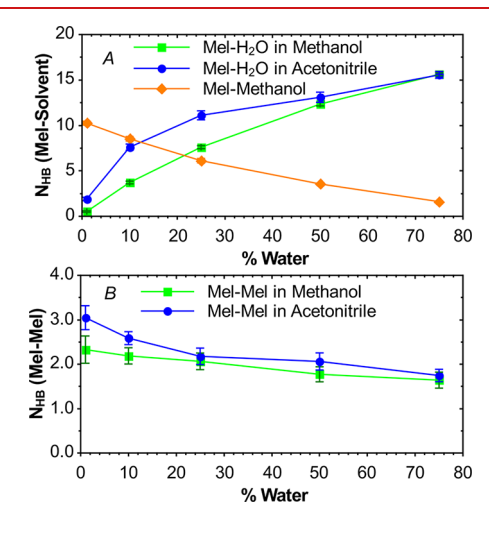


Figure 5. Average number of hydrogen bonds per time frame between melezitose and solvent, either water or methanol (A) and within melezitose molecules (B) in bulk systems with solvent mixtures of varying water composition.

The green and blue traces correspond to melezitose—water intermolecular bonds in the presence of methanol or acetonitrile, respectively. For the lowest volume percentage of water in both systems (1%), the number of intermolecular hydrogen bonds between melezitose and water per time frame is 0.5 ± 0.1 for methanol systems and 1.9 ± 0.2 for acetonitrile systems. The trend in the number of hydrogen bonds with water increases for both systems to a maximum of 18.4 ± 0.4 hydrogen bonds in 100% water (data point not shown in Figure 5).

The number of intramolecular hydrogen bonds that is formed within a melezitose molecule is presented in Figure 5B. The number of hydrogen bonds in methanol and acetonitrile systems (with 1% water) is 2.3 ± 0.3 and 3.1 ± 0.3 , respectively. The number of hydrogen bonds within melezitose is higher in acetonitrile versus methanol due to the ability of melezitose to hydrogen bond with methanol, thus forming fewer hydrogen bonds within itself. As the volume % of water increases in methanol or acetonitrile, the number of hydrogen-bonding interactions between melezitose and water increases (Figure 5A). The number of intramolecular hydrogen bonds within melezitose decreases with increasing percentage of water (Figure 5 B) and is approaching those of 100% water, which we determined in a previous study to be 1.21 hydrogen bonds per time frame.

The investigation of hydrogen bonding interactions of melezitose in bulk systems is a valuable benchmark to compare to hydrogen bond trends in evaporating droplets (Figure 6).

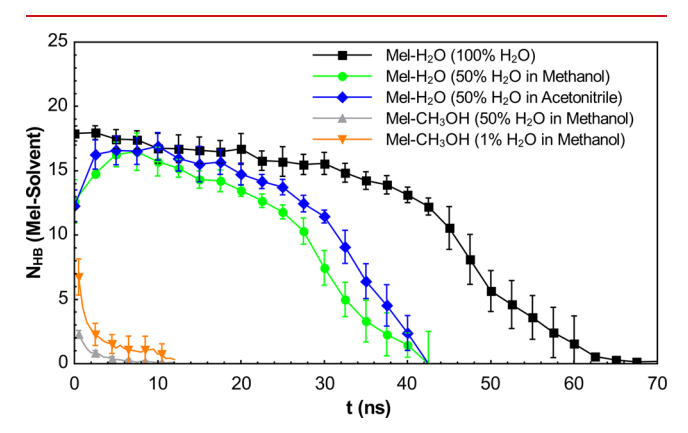


Figure 6. Time evolution of the number of hydrogen bonds between melezitose and solvent in evaporating drops with solvent mixtures of varying water composition. The points indicated are running averages of 50 trajectories.

Within evaporating droplets with 100% water (black trace), there exists an average of 17.9 ± 0.6 hydrogen bonds between melezitose and water, similar to that of bulk water, which decreases with solvent evaporation. For the hydrogen bonds between melezitose and water in evaporating droplets containing 50% water in methanol or acetonitrile (green and blue traces, respectively), the number of hydrogen bonds starts off much lower, 13 ± 2 and 12 ± 1 hydrogen bonds, respectively, and increases to a number in a range similar to 100% water.

This increase in hydrogen bonds between melezitose and water correlates to demixing, as methanol or acetonitrile molecules move to the droplet periphery, while melezitose becomes more solvated with water. The number of hydrogen bonds between melezitose and methanol is also shown (gray

and orange traces) for droplets containing 50% and 1% water in methanol, respectively. More hydrogen bonds are formed between melezitose and methanol for droplets containing 1% water than those with 50% water in methanol. The general trend is that the number of hydrogen bonds between melezitose and methanol decreases rapidly as the methanol molecules move to the surface of the droplet and evaporate.

3.4. Variation in Solvent Composition Affects Carbohydrate Conformation. Having established that the local environment of the carbohydrate will either be primarily water solvated (for most mixed compositions due to demixing) or primarily methanol or acetonitrile solvated (in 1% water compositions), we then examined the main conformational differences arising from those two environments. We monitored dihedral angles of melezitose in different solvent compositions using the gmx angle tool in GROMACS.²² Dihedral angles are the angles formed between two intersecting planes, with each plane consisting of atoms of interest. Differences in dihedral angle profiles do not arise from a change in the specific angles but are from changes in the probability distributions for particular dihedral angles, thus reflecting conformational differences. The dihedral angles monitored involved the four hydroxymethyl (CH2OH) side groups (Figure 7) as well as the dihedral angles involving glycosidic bonds and hydroxyl groups (Supporting Information Figures S4 and S5). The dihedral angle distribution profiles indicate that the structure of the carbohydrate varies in different solvent environments. The greatest variations in the dihedral angles are observed in systems with the highest

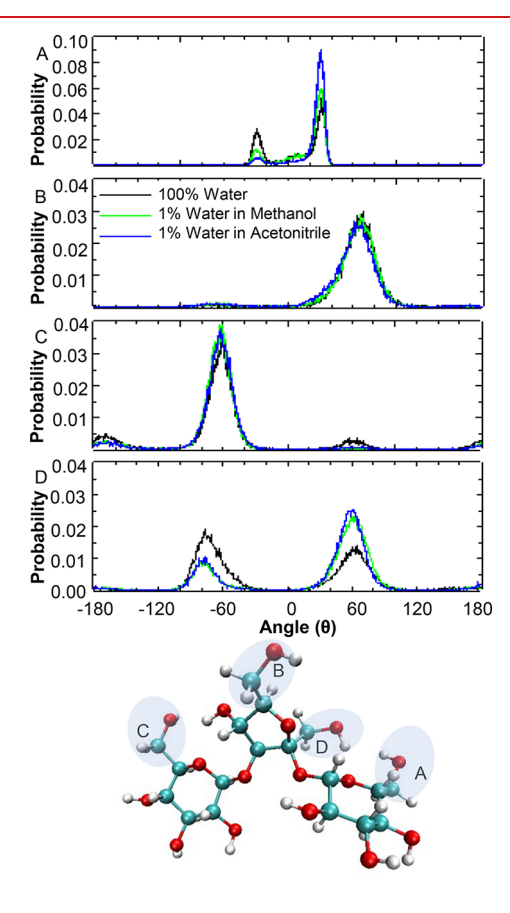


Figure 7. Probability distribution profiles for dihedral angles of CH₂OH side groups of melezitose in water (black traces), methanol (green traces), and acetonitrile (blue traces) from MD simulations.

proportion of methanol or acetonitrile (1% water) compared to 100% water, as can be seen in Figure 7A,D.

To determine whether solvent composition affects the structure of the adducts that are released into the gas phase during ESI, we also analyzed the dihedral angles of carbohydrate-metal adducts that are formed immediately after the last solvent molecule evaporates (Supporting Information Figures S6, S7, and S8). We found that there were a few similarities between 1% water droplets and 10% water droplets but saw greater differences in the dihedral angles of the adducts formed from droplets with 1% water compared to that of adducts formed from droplets with 25% or more water upon immediate desolvation. Given that the analyte is primarily solvated by water, even when up to 75% of the more volatile solvent is used, the more volatile solvent may be added to achieve greater ionization efficiency without affecting the solvated structure of the carbohydrate. However, when the concentration of methanol or acetonitrile is high (90% or more) compared to water, structural changes in the analyte, such as changes in hydrogen bonding, are expected to arise. It is important to know how differences in the ESI solvent environment affect carbohydrate structures because MS methods characterize the resulting gas-phase ions. These structural changes associated with different solvent environments were sampled for 30 ps after complete droplet desolvation. Therefore, future work should explore if these structural differences are retained as the carbohydrates pass into and through the mass spectrometer for further characterization, by IM-MS, tandem MS, or detection.

4. CONCLUSIONS

We have used MD simulations complemented with ESI-MS experiments to investigate the formation of carbohydrate-Na⁺ adducts from droplets with varying compositions of water in mixtures with methanol or acetonitrile. We observed greater ionization efficiency in mixtures with increasing percentages of organic cosolvent, owing to faster evaporative rates and increased droplet instability. We determined that the method of ionization in water/methanol or water/acetonitrile mixtures was the CRM, similar to glycans solvated with 100% water. The improved ionization was not a result of a change in the mechanism of ionization but was due to a faster evaporative rate and reduction in droplet stability. Methanol and acetonitrile experienced faster evaporation due to their greater volatility, and this evaporative rate was further enhanced by the demixing of organic solvent molecules to the droplet surface. Interactions of carbohydrates with ions, water, and cosolvent affected the release of adducts into the gas phase. This supports what we observed experimentally with greater ionization efficiency in the presence of mixed solvents. The changes in solvent around the carbohydrate affected the intermolecular hydrogen bonds with solvent and the intramolecular hydrogen bonds within the carbohydrate, itself. Based on dihedral angle analysis, the most drastic structural changes of melezitose were observed when the carbohydrate was solvated by the lowest concentrations of water. These droplets with low concentrations of water also produced gasphase ions that have structural differences compared to droplets with 25% or more water, upon immediate desolvation. Therefore, we conclude that solvent mixtures with 25% or greater proportions of water in methanol or acetonitrile are the best composition for experimental methods which use ESI to produce gas-phase ions, with minimal structural effects and

enhanced ionization. This work is the first to characterize the electrospray ionization of a model carbohydrate in solvent mixtures. It will be important to expand our investigation to carbohydrate linkage isomers since we have shown that interactions in mixed solvents affect conformational preferences of carbohydrates. Such an investigation would be crucial to determine how mixed solvents can be used to improve ion mobility and fragmentation techniques, without affecting how the results should be interpreted for isomer characterization.

ASSOCIATED CONTENT

Solution Supporting Information

The Supporting Information is available free of charge at https://pubs.acs.org/doi/10.1021/jasms.1c00179.

Snapshots of MD simulations showing solvent distributions in droplets at different evaporation stages for methanol (S1) and acetonitrile (S2) systems; Plots of coordination numbers between melezitose and sodium ions (S3); Probability distribution profiles for dihedral angles of solvated melezitose involving glycosidic bonds (S4) and hydroxyl groups (S5); Probability distribution profiles for dihedral angles of gas-phase melezitose—Na⁺ adducts involving glycosidic bonds (S6), CH₂OH side groups (S7), and hydroxyl groups (S8) (PDF)

AUTHOR INFORMATION

Corresponding Author

Elyssia S. Gallagher — Department of Chemistry and Biochemistry, Baylor University, Waco, Texas 76798-7348, United States; Occid.org/0000-0002-5411-7285; Email: elyssia gallagher@baylor.edu

Authors

Emvia I. Calixte – Department of Chemistry and Biochemistry, Baylor University, Waco, Texas 76798-7348, United States

O. Tara Liyanage — Department of Chemistry and Biochemistry, Baylor University, Waco, Texas 76798-7348, United States; orcid.org/0000-0002-1121-2485

Darren T. Gass – Department of Chemistry and Biochemistry, Baylor University, Waco, Texas 76798-7348, United States

Complete contact information is available at: https://pubs.acs.org/10.1021/jasms.1c00179

Notes

The authors declare no competing financial interest.

ACKNOWLEDGMENTS

We acknowledge financial support from The Welch Foundation: AA-1899 and the National Science Foundation: CHE-1945078. We thank the Baylor University Supercomputing Center for use of the high-performance cluster (Kodiak) and the Baylor University Mass Spectrometry Center. We gratefully acknowledge Dr. Lars Konermann for the use of his evaporation code.

REFERENCES

(1) Lau, K. S.; Partridge, E. A.; Grigorian, A.; Silvescu, C. I.; Reinhold, V. N.; Demetriou, M.; Dennis, J. W. Complex N-Glycan Number and Degree of Branching Cooperate to Regulate Cell Proliferation and Differentiation. *Cell* **2007**, *129* (1), 123–134.

- (2) Essentials of Glycobiology, 2nd ed.; Cold Spring Harbor Laboratory Press: Cold Spring Harbor (NY), 2009.
- (3) An, H. J.; Kronewitter, S. R.; de Leoz, M. L. A.; Lebrilla, C. B. Glycomics and disease markers. *Curr. Opin. Chem. Biol.* **2009**, *13* (5–6), 601–607.
- (4) Mucha, E.; Stuckmann, A.; Marianski, M.; Struwe, W. B.; Meijer, G.; Pagel, K. In-depth structural analysis of glycans in the gas phase. *Chem. Sci.* **2019**, *10* (5), 1272–1284.
- (5) Kailemia, M. J.; Ruhaak, L. R.; Lebrilla, C. B.; Amster, I. J. Oligosaccharide Analysis by Mass Spectrometry: A Review of Recent Developments. *Anal. Chem.* **2014**, *86* (1), 196–212.
- (6) Kostyukevich, Y.; Kononikhin, A.; Popov, I.; Nikolaev, E. In-ESI Source Hydrogen/Deuterium Exchange of Carbohydrate Ions. *Anal. Chem.* **2014**, *86* (5), 2595–2600.
- (7) Liyanage, O. T.; Brantley, M. R.; Calixte, E. I.; Solouki, T.; Shuford, K. L.; Gallagher, E. S. Characterization of Electrospray Ionization (ESI) Parameters on In-ESI Hydrogen/Deuterium Exchange of Carbohydrate-Metal Ion Adducts. *J. Am. Soc. Mass Spectrom.* **2019**, 30 (2), 235–247.
- (8) Thacker, J. B.; Schug, K. A. Effects of solvent parameters on the electrospray ionization tandem mass spectrometry response of glucose. *Rapid Commun. Mass Spectrom.* **2018**, 32 (15), 1191–1198.
- (9) Jemal, M.; Hawthorne, D. J. Effect of high performance liquid chromatography mobile phase (methanol versus acetonitrile) on the positive and negative ion electrospray response of a compound that contains both an unsaturated lactone and a methyl sulfone group. *Rapid Commun. Mass Spectrom.* **1999**, *13* (1), 61–66.
- (10) McAllister, R. G.; Metwally, H.; Sun, Y.; Konermann, L. Release of Native-like Gaseous Proteins from Electrospray Droplets via the Charged Residue Mechanism: Insights from Molecular Dynamics Simulations. J. Am. Chem. Soc. 2015, 137 (39), 12667—12676
- (11) Calixte, E. I.; Liyanage, O. T.; Kim, H. J.; Ziperman, E. D.; Pearson, A. J.; Gallagher, E. S. Release of Carbohydrate—Metal Adducts from Electrospray Droplets: Insight into Glycan Ionization by Electrospray. *J. Phys. Chem. B* **2020**, *124* (3), 479–486.
- (12) Porrini, M.; Rosu, F.; Rabin, C.; Darré, L.; Gómez, H.; Orozco, M.; Gabelica, V. Compaction of Duplex Nucleic Acids upon Native Electrospray Mass Spectrometry. ACS Cent. Sci. 2017, 3 (5), 454–461.
- (13) Hao, D.; Yang, Z.; Gao, T.; Tian, Z.; Zhang, L.; Zhang, S. Role of glycans in cholesteryl ester transfer protein revealed by molecular dynamics simulation. *Proteins: Struct., Funct., Genet.* **2018**, *86* (8), 882–891.
- (14) Rönnols, J.; Engström, O.; Schnupf, U.; Säwén, E.; Brady, J. W.; Widmalm, G. Inter-residual Hydrogen Bonding in Carbohydrates Unraveled by NMR Spectroscopy and Molecular Dynamics Simulations. *ChemBioChem* **2019**, 20 (19), 2519–2528.
- (15) Konermann, L.; McAllister, R. G.; Metwally, H. Molecular Dynamics Simulations of the Electrospray Process: Formation of NaCl Clusters via the Charged Residue Mechanism. *J. Phys. Chem. B* **2014**, *118* (41), 12025–12033.
- (16) Konermann, L.; Ahadi, E.; Rodriguez, A. D.; Vahidi, S. Unraveling the Mechanism of Electrospray Ionization. *Anal. Chem.* **2013**, *85* (1), 2–9.
- (17) Sterling, T.; Irwin, J. J. ZINC 15 Ligand Discovery for Everyone. J. Chem. Inf. Model. 2015, 55 (11), 2324–2337.
- (18) Frisch, M. J.; Trucks, G. W.; Schlegel, H. B.; Scuseria, G. E.; Robb, M. A.; Cheeseman, J. R.; Scalmani, G.; Barone, V.; Petersson, G. A.; Nakatsuji, H. *Gaussian 09*, Revision C.01; Gaussian: Wallingford, CT, 2009.
- (19) Guvench, O.; Mallajosyula, S. S.; Raman, E. P.; Hatcher, E.; Vanommeslaeghe, K.; Foster, T. J.; Jamison, F. W.; MacKerell, A. D. CHARMM Additive All-Atom Force Field for Carbohydrate Derivatives and Its Utility in Polysaccharide and Carbohydrate—Protein Modeling. J. Chem. Theory Comput. 2011, 7 (10), 3162–3180.
- (20) Vanommeslaeghe, K.; Hatcher, E.; Acharya, C.; Kundu, S.; Zhong, S.; Shim, J.; Darian, E.; Guvench, O.; Lopes, P.; Vorobyov, I.; Mackerell Jr, A. D. CHARMM general force field: A force field for

- drug-like molecules compatible with the CHARMM all-atom additive biological force fields. *J. Comput. Chem.* **2009**, 31 (4), 671–690.
- (21) Vanommeslaeghe, K.; Raman, E. P.; MacKerell, A. D., Jr. Automation of the CHARMM General Force Field (CGenFF) II: assignment of bonded parameters and partial atomic charges. *J. Chem. Inf. Model.* **2012**, *52* (12), 3155–3168.
- (22) Hess, B.; Kutzner, C.; van der Spoel, D.; Lindahl, E. GROMACS 4: Algorithms for Highly Efficient, Load-Balanced, and Scalable Molecular Simulation. *J. Chem. Theory Comput.* **2008**, *4* (3), 435–447.
- (23) Iribarne, J. V.; Thomson, B. A. On the evaporation of small ions from charged droplets. *J. Chem. Phys.* **1976**, *64* (6), 2287–2294.
- (24) Martínez, L.; Andrade, R.; Birgin, E. G.; Martínez, J. M. PACKMOL: A package for building initial configurations for molecular dynamics simulations. *J. Comput. Chem.* **2009**, *30* (13), 2157–2164.
- (25) Rayleigh, L. On the equilibrium of liquid conducting masses charged with electricity. *Philos. Mag.* **1882**, *14* (87), 184–186.
- (26) Vazquez, G.; Alvarez, E.; Navaza, J. M. Surface Tension of Alcohol + Water from 20 to 50 °C. *J. Chem. Eng. Data* **1995**, 40 (3), 611–614.
- (27) Weast, R. C. CRC handbook of chemistry and physics, 1st Student ed.; CRC Press: Boca Raton, FL, 1988.
- (28) Konermann, L.; Metwally, H.; McAllister, R. G.; Popa, V. How to Run Molecular Dynamics Simulations on Electrospray Droplets and Gas Phase Proteins: Basic Guidelines and Selected Applications. *Methods* **2018**, *144*, 104–112.
- (29) Hockney, R. W.; Goel, S. P.; Eastwood, J. W. Quiet high-resolution computer models of a plasma. *J. Comput. Phys.* **1974**, *14* (2), 148–158.
- (30) Verlet, L. Computer "Experiments" on Classical Fluids. I. Thermodynamical Properties of Lennard-Jones Molecules. *Phys. Rev.* **1967**, *159* (1), 98–103.
- (31) Nosé, S. A molecular dynamics method for simulations in the canonical ensemble. *Mol. Phys.* **1984**, *52* (2), 255–268.
- (32) Hoover, W. G. Canonical dynamics: Equilibrium phase-space distributions. *Phys. Rev. A: At., Mol., Opt. Phys.* **1985**, 31 (3), 1695–1697.
- (33) Konermann, L.; Metwally, H.; McAllister, R. G.; Popa, V. How to run molecular dynamics simulations on electrospray droplets and gas phase proteins: Basic guidelines and selected applications. *Methods* **2018**, *144*, 104–112.
- (34) Schlesinger, D.; Sellberg, J. A.; Nilsson, A.; Pettersson, L. G. M. Evaporative cooling of microscopic water droplets in vacuo: Molecular dynamics simulations and kinetic gas theory. *J. Chem. Phys.* **2016**, *144* (12), 124502.
- (35) Ahadi, E.; Konermann, L. Ejection of Solvated Ions from Electrosprayed Methanol/Water Nanodroplets Studied by Molecular Dynamics Simulations. *J. Am. Chem. Soc.* **2011**, *133* (24), 9354–9363.